J. Phys.: Condens. Matter **21** (2009) 134019 (6pp) doi:10.1088/0953-8984/21/13/134019

Morphology and CO adsorption on platinum supported on thin $Fe_3O_4(111)$ films

Z-H Qin, M Lewandowski, Y-N Sun, S Shaikhutdinov[1] and H-J Freund

Abteilung Chemische Physik, Fritz-Haber-Institut der Max-Planck-Gesellschaft, Faradayweg 4-6, Berlin 14195, Germany

E-mail: shaikhutdinov@fhi-berlin.mpg.de

Received 2 October 2008, in final form 30 October 2008
Published 12 March 2009
Online at stacks.iop.org/JPhysCM/21/134019

Abstract

Nucleation, growth and thermal stability of Pt particles supported on well ordered $Fe_3O_4(111)$ thin films grown on Pt(111) were studied by scanning tunnelling microscopy (STM) and temperature programmed desorption (TPD) of CO. STM studies showed that Pt grows through the formation of single-layer islands that coalesce at high coverage. Vacuum annealing at 600 K caused Pt sintering and the formation of extended two-dimensional (2D) islands one and two layers in thickness at sub-monolayer coverage. Well faceted, three-dimensional (3D) Pt nanoparticles formed by annealing to temperatures above 800 K were encapsulated by an FeO(111) monolayer. These results were rationalized in terms of the high adhesion energy for Pt on iron oxide surfaces. CO TPD studies showed that 2D structures, formed at 600 K, exhibit much lower CO adsorption capacity as compared to the Pt(111) single crystal surface. This effect has been tentatively assigned to lattice expansion in the Pt 2D islands leading to weakening of the Pt–CO bond due to reduction of the Pt $\rightarrow$ CO π^* back-donation.

(Some figures in this article are in colour only in the electronic version)

1. Introduction

Platinum group metals supported on oxides are widely used in many industrially important catalytic processes. To elucidate the mechanism of reactions on a molecular level, various model systems have been suggested where metal particles are deposited onto crystalline oxide surfaces of single crystals and well ordered thin films [1–3]. In particular, structure and reactivity of the Pt particles supported on transition metal oxides such as $TiO_2(110)$ and $CeO_2(111)$ have been studied quite intensively using 'surface science' methods [4–9]. Less is known about the interaction of platinum metals with iron oxide surfaces. For instance, growth of Pt, Ag and Au nm thick films on Fe_3O_4 substrates was studied by high energy electron diffraction and transmission electron microscopy [10, 11], which revealed epitaxial relationships between the metals and the iron oxide. The structure of Pd particles on well ordered $Fe_3O_4(111)$ films has been studied in our group [12–16]. In particular, an interface oxide layer between Pd and Fe_3O_4 was observed upon oxidation at 500–550 K, which in turn affected the kinetics of the CO oxidation reaction.

The termination of the close-packed surfaces of iron oxides has been addressed by Weiss and Ranke in their review [17]. In particular, it has been suggested that the $Fe_3O_4(111)$ surface is terminated by 1/4 ML of Fe cations. However, this surface structure is still debated in the literature [18–20], and it seems to strongly depend on preparation conditions.

Very recently, we have reported that Pt nanoparticles supported on $Fe_3O_4(111)$ films exhibit the so-called strong metal–support interaction (SMSI) [21] that leads to the encapsulation of Pt particles by an FeO(111) monolayer [22]. In this paper, we present a systematic study of the growth, thermal stability and CO adsorption properties of Pt particles supported on $Fe_3O_4(111)$ films using scanning tunnelling microscopy (STM) and temperature programmed desorption (TPD).

[1] Author to whom any correspondence should be addressed.

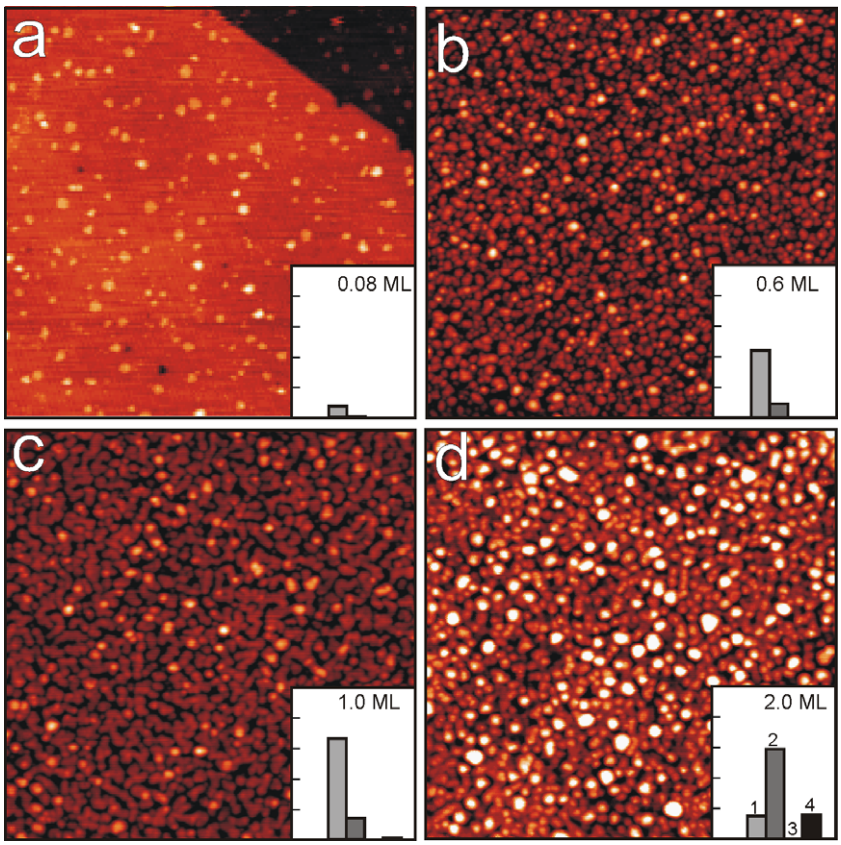

Figure 1. Room temperature STM images (100 nm × 100 nm) of Pt deposited on the $Fe_3O_4(111)$ films at ∼110 K at the Pt coverage as indicated. At the low coverage, the Pt islands are mostly one Pt(111) layer in height. The insets show a normalized particle height histogram indicated in numbers of (111) layers as indicated in the inset (d).

2. Experimental details

The experiments were performed in an ultra-high vacuum (UHV) chamber (base pressure below 3×10^{-10} mbar) equipped with low energy diffraction/Auger electron spectroscopy (LEED/AES, Specs), STM (Omicron) and a differentially pumped quadrupole mass spectrometer (QMS, Fision) for TPD measurements. The Pt(111) crystal (99.95% from Mateck, ∼10 mm in diameter, 2 mm thick) was mounted on the sample holder and could be heated by electron bombardment from the backside using a W filament. The temperature was measured with a chromel–alumel thermocouple spot-welded to the edge of the crystal. The crystal temperature was controlled using a feedback system (Schlichting Phys. Instrum.).

The $Fe_3O_4(111)$ films were grown on a Pt(111) substrate as described in detail in [16, 17, 20, 22]. Briefly, about one monolayer (1 ML = 1.3×10^{15} at cm^{-2}) of Fe was evaporated onto clean Pt(111) at 300 K and subsequently oxidized in 10^{-6} mbar O_2 at 1000 K for 2 min to form the FeO(111) monolayer film. The ∼10 nm thick $Fe_3O_4(111)$ films were grown by repeated cycles of ∼5 ML Fe deposition and oxidation at ∼900 K with the final oxidation step at ∼1000 K for 10 min. Prior to Pt deposition, the $Fe_3O_4(111)$ films were flashed to $T > 800$ K in UHV, thus resulting in a single termination oxide surface as judged by STM.

Iron and Pt (both 99.95%, Goodfellow) were deposited using commercial evaporators (Focus EFM3, Omicron). During deposition, the sample was biased with a retarding potential to prevent metal ions from being accelerated towards the sample.

The STM images presented here were obtained with commercial Pt–Ir tips (LOT Oriel GmbH) at tunnelling currents of 0.6–1 nA and positive sample bias of 1–1.4 V. To obtain atomic resolution the bias was lowered to ∼0.5 V.

3. Results and discussion

Figure 1(a) shows a room temperature STM image of Pt deposited on an $Fe_3O_4(111)$ film at the lowest coverage studied, i.e. 0.08 ML. The Pt particles with a rather broad lateral size distribution are randomly dispersed on the terrace with almost no decoration of the step edges, thus indicating relatively strong interaction of the Pt ad-atoms with the regular oxide surface. This is also consistent with the fact that most of the particles are about 0.3 nm in height, that is close to a single atomic layer of Pt, which is 0.23 nm in Pt(111). Certainly, an apparent height measured for metal particles deposited on oxide substrates may depend on the tunnelling parameters. Therefore, the assignment to monolayer islands was also made based on Pt coverage calibrated by STM on Pt islands formed on Pt(111).

Upon increasing the coverage to 0.6 ML, the particle density increased remarkably; however, their average size

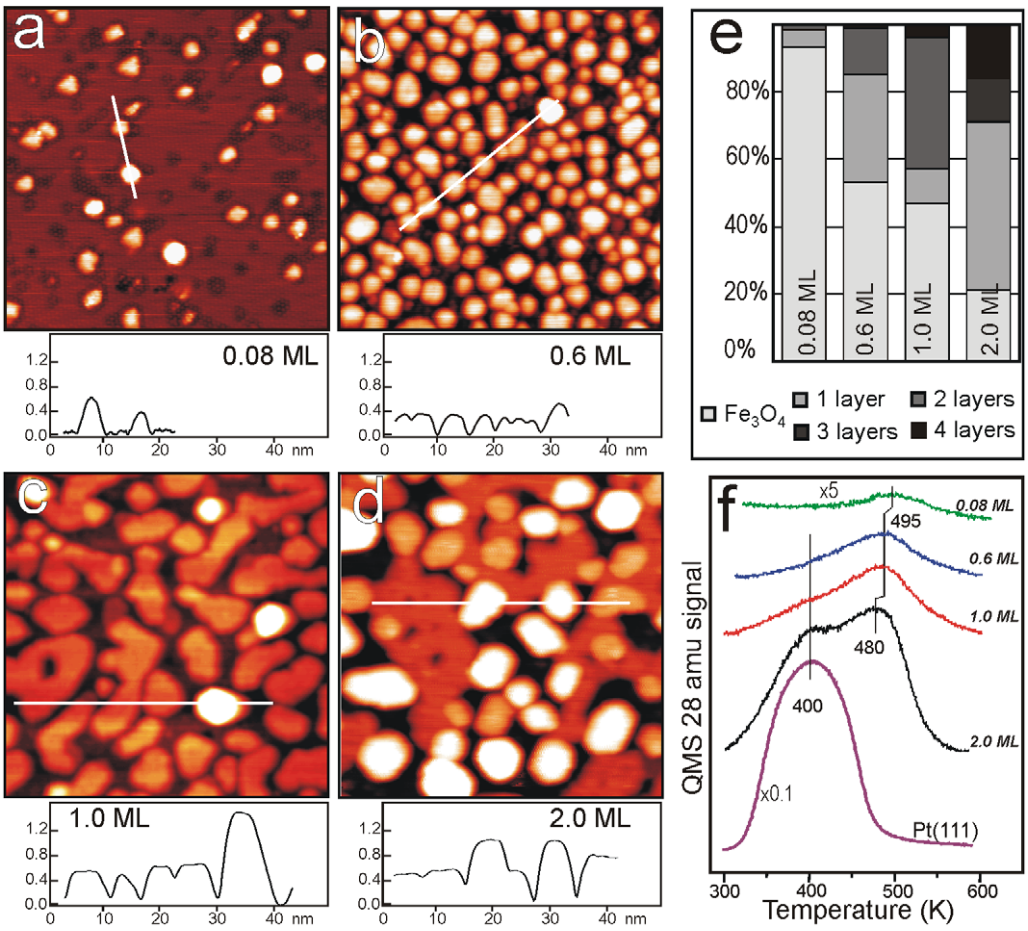

Figure 2. (a)–(d) STM images (50 nm × 50 nm) of the samples shown in figure 1 after subsequent annealing at 600 K for 1 min. Height profiles along the lines are shown below each image. Panel (e) shows each particle's height distribution. TPD spectra of 5 L CO adsorbed at 300 K are shown in (f). The spectrum from the Pt(111) crystal is also shown, for comparison. The spectra are offset for clarity.

(∼2 nm) and height remained basically unchanged (see figure 1(b)). The particles coalesced and formed extended, irregularly shaped two-dimensional (2D) islands covering ∼2/3 of the support as the total Pt coverage increased to 1 ML (figure 1(c)). Further increase of the coverage to 2 ML resulted in a surface mostly covered by particles of ∼0.5 nm in height, which is approximately double of the value measured at lower coverages, and therefore are assigned to two monolayers islands (figure 1(d)). Coverage dependent changes in the height distribution of the particles can be monitored by the insets in figure 1 showing that the portion of multilayer particles increases with increasing Pt coverage.

Certainly, the growth of the Pt particles by deposition at 100 K (and heating to 300 K for STM studies) may be a kinetically limited process, resulting in non-equilibrium particle size and shape. To see whether the formation of monolayer islands is thermodynamically driven, the samples were annealed at 600 K for 1 min, as shown in figure 2. While no significant changes were observed at 0.08 ML, annealing obviously caused Pt sintering at higher coverage. Interestingly, monolayer islands still dominate the structure at 0.6 ML while their sizes increased by factor of two (figure 2(b)). At 1 ML coverage, islands were primarily two monolayers in thickness and exhibited mostly irregular shape, although some preferential orientation of the island edges can be seen in figure 2(c). At the highest coverage studied (2 ML, see figure 2(d)), three-dimensional (3D) particles up to 1 nm in height were observed in addition to extended 2D islands. The diagram in figure 2(e) summarizes height distributions of Pt particles in the annealed samples.

It has previously been shown that under the same conditions Pd forms only well faceted 3D particles on $Fe_3O_4(111)$ [13, 16]. Since the surface energy of Pt is higher than that of Pd [23], which would form even more 3D particles, the formation of Pt 2D structures implies a higher work of adhesion (W_{adh}), which is defined through the corresponding surface energies (γ) as $W_{adh} = \gamma_{oxide} + \gamma_{metal} - \gamma_{interface}$. This energy can be derived from the structural information provided by STM on the basis of the Wulff construction [24, 25]. The analysis applied to 2D islands, which presumably reached equilibrium structures by annealing at 600 K for 1 min (see figure 2(c)), resulted in $W_{adh} = 4.0 \pm 0.5$ J m^{-2} by using the theoretical value of 2.3 J m^{-2} for $\gamma_{Pt(111)}$ [23]. For the 3D particles imaged in figure 2(d), the analysis gave $W_{adh} = 3.8 \pm 0.1$ J m^{-2}. Both numbers are significantly larger than the 3.15 ± 0.1 J m^{-2} obtained for $Pd/Fe_3O_4(111)$ at 600 K, and the 3.25 ± 0.3 J m^{-2} previously reported for Pd on thin alumina films at 300 K [25], using the γ values for Pd(111)

and Pt(111) from the DFT calculations of the same group [23] for comparison. Therefore, this analysis indicates that the high adhesion energy between Pt and $Fe_3O_4(111)$ favours the formation of 2D structures.

The surface structure of Pt particles was further examined by TPD of CO as a probe molecule. Figure 2(f) presents CO TPD spectra of the samples shown in figures 2(a)–(d). Note that CO on the clean $Fe_3O_4(111)$ support fully desorbs at temperatures below 250 K [16, 20] and, therefore, does not contribute to the spectra. At sub-monolayer Pt coverage, CO desorbs in a broad peak centred at ∼495 K with a small shoulder at ∼400 K. Increasing the coverage to 2 ML shifts the high temperature peak to ∼480 K and the signal at ∼400 K gains intensity. The low temperature signal resembles the one measured with the same experimental set-up on the Pt(111) single crystal used as a substrate for the oxide film. The desorption signals at ∼400 and ∼480 K are usually rationalized as CO adsorbing on Pt(111) terraces and low-coordination sites (such as steps, kinks and particle edges), respectively [26–29]. However, the cross-analysis of STM and TPD data presented in figure 2 revealed some interesting CO adsorption behaviour, as discussed below.

First we address the morphology of the Pt deposits. Since well ordered FeO(111) and $Fe_3O_4(111)$ thin films can be grown on Pt(111), one would also expect that Pt particles on $Fe_3O_4(111)$ also grow in the (111) direction. Indeed, diffraction studies showed good epitaxial relationships between Pt and Fe_3O_4, such that the top facets of Pt on $Fe_3O_4(111)$ expose Pt(111) [10, 11]. (Basically, the same epitaxy was observed for Pd, having almost identical lattice constant to Pt [12, 16].) Therefore, we may conclude that the sample possessing 1 ML of Pt is covered by Pt(111) islands which are primarily two layers in thickness (see figure 2(c)). These islands are relatively large (∼10 nm in width, on average); therefore, the contribution of Pt sites on the island's brim versus the total CO adsorption is rather small. However, the corresponding TPD spectrum in figure 2(f) clearly shows a signal at ∼490 K (i.e. assigned to low coordinated sites), but almost no signal at ∼400 K (i.e. characteristic for Pt(111)). While the intensity of the high temperature peak scales with Pt coverage in the sub-monolayer regime (where only 2D structures are observed, see figures 2(a)–(c)), the desorption peak at ∼400 K has been resolved only on the 2 ML sample, where 3D nanoparticles start to grow (see figure 2(d)).

Furthermore, CO uptake per Pt surface area measured on the 1 ML sample turned out to be ∼10 times lower than on the Pt(111) crystal. This ratio increases even more if one only considers the TPD area under the signal centred at 400 K following a spectral deconvolution. Note that the islands are large enough to neglect, in the first approximation, the reduction of the effective Pt(111) surface by adsorption sites at the island periphery. Finally, TPD spectra of CO adsorbed at 100 K (not shown here) on samples similarly prepared in another UHV chamber nicely reproduced the coverage dependent results of CO adsorption at 300 K. At temperatures between 100 and 300 K, the TPD spectra revealed desorption peaks characteristic for the pristine iron oxide support, which might obscure observation of signals (if any) coming from Pt islands, but no new features were detected. Therefore, combined STM and TPD results suggest that the mono- and bilayer Pt(111) structures formed on $Fe_3O_4(111)$, at least, do not adsorb CO in the same fashion as the 3D particles and Pt(111) crystal surface, or may even be inert to CO at temperatures above ∼100 K.

The origin of this effect is unclear. One could argue that the 2D islands seen in STM exposed not a clean Pt surface but, for example, an alloy of Pt with iron oxide or Pt encapsulated by iron oxide. However, CO TPD spectra from the samples 'as prepared' at ∼100 K, where encapsulation and alloy formation is hardly possible, showed similar desorption spectra with only ∼30% higher CO uptake as compared to that of the sample annealed to 600 K. The latter finding can be readily explained by Pt sintering and coalescence upon heating from 100 to 600 K.

To rationalize the unusual CO adsorption properties of the 2D islands, we have assumed that both mono- and two-layer Pt(111) islands adopt the structure of an $Fe_3O_4(111)$ surface underneath. In other words, the Pt lattice constant is expanded from 0.277 to 0.297 nm [17]. In principle, this assumption would be consistent with the high adhesion energy between Pt and iron oxide as discussed above. In addition, we did not find Pt(111) spots or streaks around integer spots of $Fe_3O_4(111)$ in the LEED pattern, which would have been expected for the sample that was ∼50% covered by extended 2D islands (see figure 2(d)). There is not so much in the literature about the effect of lattice strain on chemisorption. Surface structures driven by lattice strain have been invoked by Bertolini and co-workers while discussing the catalytic properties of bimetallic surfaces in hydrogenation reactions ([30] and references therein). Other research groups explain downward shift in CO adsorption on bimetallic surfaces in terms of changes in the electronic structure (see reviews [31, 32]). For the first time the importance of the lattice strain in the electronic structure of metal nanoparticles has been addressed in the paper of Richter *et al* [33]. Based on the Blyholder model of CO adsorption on metals [34], the lattice expansion will reduce Pt → CO π^* back-donation and therefore weaken the Pt–CO bond. However, more elaborate theoretical studies are necessary to validate this hypothesis.

We have also examined the thermal stability of the Pt deposits at elevated temperatures. Figure 3 shows STM images of the 2.6 ML Pt sample as deposited at 300 K (a), after flashing to 600 K (b), after annealing at 600 K for 5 min (c) and finally after annealing at 850 K for 1 min (d). The diagram in figure 3(f) shows height distributions of the Pt particles after each treatment. It is clear that annealing causes Pt dewetting such that the particles become higher with increasing annealing temperature. Concomitantly, the uncovered support area increases. The particles become better shaped, with their edges running along the main crystallographic directions of $Fe_3O_4(111)$ imaged with atomic resolution between the particles. These results confirm the epitaxial relationship $Pt(111)[1\bar{1}0] \parallel Fe_3O_4(111)[1\bar{1}0]$ found by diffraction methods [10, 11], whereby the particles expose top (111) facets.

The corresponding CO TPD spectra are shown in figure 3(e). Compared to the spectra presented in figure 2(f),

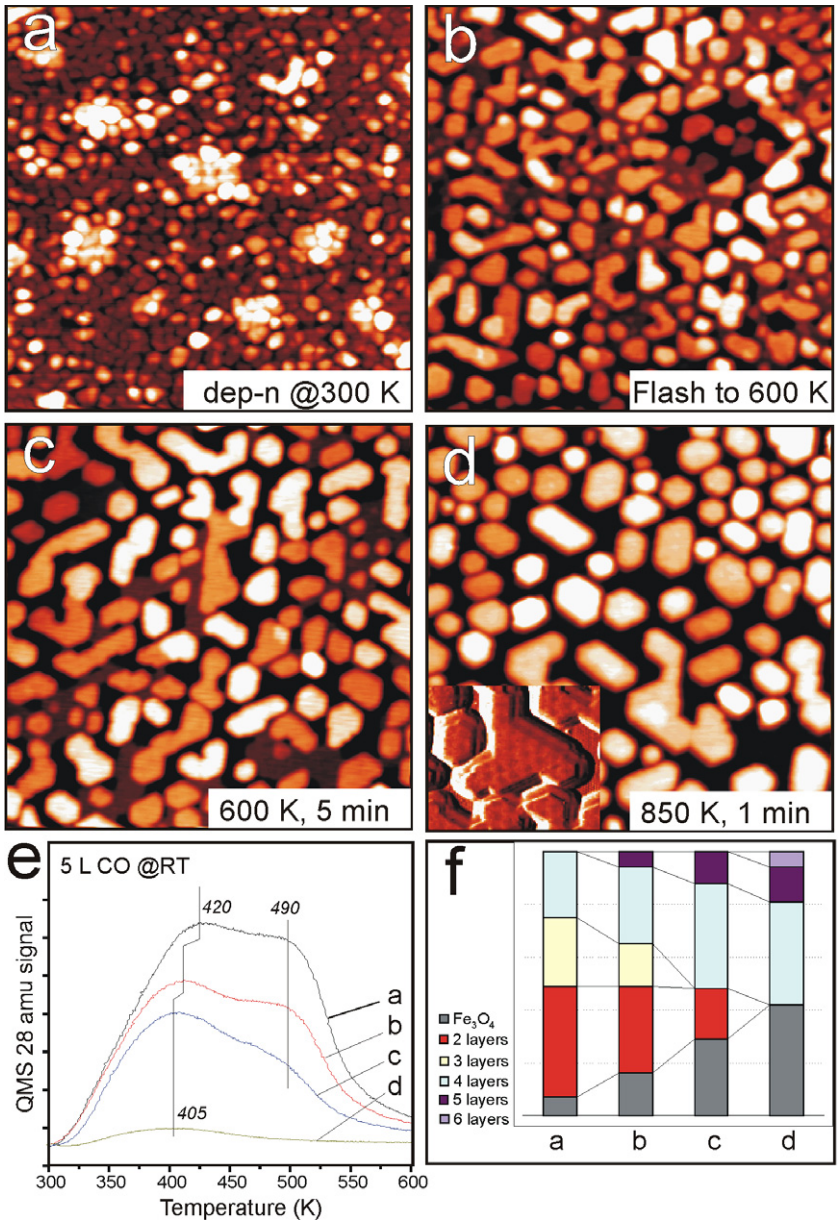

Figure 3. STM images (100 nm × 100 nm) of a 2.6 ML Pt/Fe_3O_4(111) sample as deposited at 300 K (a) and after flashing to 600 K (b) and annealing at 600 K for 5 min (c) and at 850 K for 1 min (d). Particles' height distribution for each sample (a)–(d) is shown in (f). The CO TPD spectra from these samples are shown in (e) as indicated. The inset in (f) shows a high resolution image presented with differentiated contrast in order to show moiré superstructure with 2.6 nm periodicity observed on the top facets due to the formation of an FeO encapsulating layer.

an increase of the 'bulk' Pt(111) component (i.e. at ∼410 K) is due to the enhanced formation of 3D particles at increasing Pt coverage. Gradual decrease of the CO adsorption capacity after thermal flash and annealing at 600 K can be explained by the reduction of Pt surface area upon sintering. However, surface area changes cannot explain the drop in CO uptake after heating to 850 K. The suppression of CO adsorption is a typical manifestation of the SMSI effect, in most cases associated with decoration of metal particles by the oxide support [21]. Indeed, the inset in figure 3(f) shows that the top facets exhibit a superstructure with an ∼2.6 nm periodicity which is identical to the moiré pattern observed for an FeO(111) monolayer film on Pt(111) [35]. Moreover, the total particle volume measured from STM images turned out to be relatively constant at 300 and 600 K, but showed an ∼20% increase upon heating to 850 K. Again, this finding supports the conclusion of Pt particle encapsulation by an oxide layer.

4. Summary and conclusions

In this paper, we have studied nucleation, growth and thermal stability of Pt particles supported on well ordered Fe_3O_4(111) thin films grown on Pt(111) using STM and CO TPD. The STM studies showed that Pt grows two-dimensionally, i.e. through the formation of single-layer islands which coalesce at increasing coverage. Vacuum annealing at 600 K caused Pt sintering and formation of extended 2D islands of

one and two layers in thickness at sub-monolayer coverage. Well faceted 3D nanoparticles were formed at annealing temperatures above 800 K; however, they were encapsulated by a FeO(111) monolayer as a result of SMSI. The results have been rationalized in terms of the high adhesion energy for Pt on iron oxide surface, i.e. about 4 J m^{-2}, which is significantly higher than the values observed for Pd particles on Fe_3O_4(111) and thin alumina films, where 3D growth from the onset has previously been observed. Cross-analysis of STM and TPD data revealed that the Pt(111) islands of two layers in thickness exhibit much lower CO uptake per Pt surface area as compared to the Pt(111) single crystal surface. The effect has been tentatively assigned to lattice expansion in Pt 2D islands that leading to weakening of the Pt–CO bond due to reduction of the Pt $\rightarrow$ CO π^* back-donation.

Acknowledgments

We thank the Cluster of Excellence UNICAT funded by the Deutsche Forschungsgemeinschaft and coordinated by the Technical University Berlin, and also the Fonds der Chemischen Industrie for financial support.

References

[1] Gunter P L J, Niemantsverdriet J W, Ribeiro F and Somorjai G 1997 *Catal. Rev. Sci. Eng.* **39** 77
[2] Goodman D W 1995 *Chem. Rev.* **95** 523
[3] Freund H-J 2002 *Surf. Sci.* **500** 271
[4] Pesty F, Steinrück H-P and Madey T E 1995 *Surf. Sci.* **339** 83
[5] Cosandey F, Zhang L and Madey T E 2001 *Surf. Sci.* **474** 1
[6] Dulub O, Hebenstreit W and Diebold U 2000 *Phys. Rev. Lett.* **84** 3646
[7] Jennison D R, Dulub O, Hebenstreit W and Diebold U 2001 *Surf. Sci.* **492** L677
[8] Gao Y, Liang Y and Chambers S A 1996 *Surf. Sci.* **365** 638
[9] Mullins D R and Zhang K Z 2002 *Surf. Sci.* **513** 163
[10] Gatel C and Snoeck E 2007 *Surf. Sci.* **601** 1031
[11] Gatel C and Snoeck E 2006 *Surf. Sci.* **600** 2650
[12] Schalow T, Brandt B, Laurin M, Schauermann S, Guimond S, Kuhlenbeck H, Libuda J and Freund H-J 2006 *Surf. Sci.* **600** 2528
[13] Schalow T, Brandt B, Starr D E, Laurin M, Schauermann S, Shaikhutdinov S K, Libuda J and Freund H-J 2006 *Catal. Lett.* **107** 189
[14] Schalow T, Brandt B, Laurin M, Schauermann S, Libuda J and Freund H-J 2006 *J. Catal.* **242** 58
[15] Schalow T, Brandt B, Starr D E, Laurin M, Shaikhutdinov S K, Schauermann S, Libuda J and Freund H-J 2006 *Angew. Chem.* **118** 3775
[16] Meyer R, Shaikhutdinov S K and Freund H-J 2004 *Z. Phys. Chem.* **218** 905
[17] Weiss W and Ranke W 2002 *Prog. Surf. Sci.* **70** 1
[18] Cutting R S, Muryn C A, Vaughan D J and Thornton G 2008 *Surf. Sci.* **602** 1155
[19] Zhu L, Yao K L and Liu Z L 2006 *Phys. Rev.* B **74** 035409
[20] Lemire C, Henrich V, Shaikhutdinov S and Freund H-J 2004 *Surf. Sci.* **572** 103
[21] Tauster S J, Fung S C and Garten R L 1978 *J. Am. Chem. Soc.* **100** 170
[22] Qin Z-H, Lewandowski M, Sun Y-N, Shaikhutdinov S and Freund H-J 2008 *J. Phys. Chem.* C **112** 10209
[23] Vitos L, Ruban A, Skriver H and Kollár J 1998 *Surf. Sci.* **411** 186
[24] Wulff G Z 1901 *Kristallografiya* **34** 449
[25] Hansen K H, Worren T, Stempel S, Lægsgaard E, Bäumer M, Freund H-J, Besenbacher F and Stensgaard I 1999 *Phys. Rev. Lett.* **83** 4120
[26] McCabe R W and Schmidt L D 1977 *Surf. Sci.* **66** 101
[27] Ertl G, Neumann M and Streit K M 1977 *Surf. Sci.* **64** 393
[28] Steiniger H, Lehwald S and Ibach H 1982 *Surf. Sci.* **123** 264
[29] Mcclellan M R, Gland J L and McFesly F R 1981 *Surf. Sci.* **112** 63
[30] Bertolini J-C 2008 *Catal. Today* **138** 84
[31] Chen J G, Menning C A and Zellner M B 2008 *Surf. Sci. Rep.* **63** 210
[32] Rodriguez J 1996 *Surf. Sci. Rep.* **24** 191
[33] Richter B, Kuhlenbeck H, Freund H-J and Bagus P S 2004 *Phys. Rev. Lett.* **93** 026805
[34] Blyholder G 1964 *J. Phys. Chem.* **68** 2772
[35] Ritter M, Ranke W and Weiss W 1998 *Phys. Rev.* B **57** 7240